



# Design of Magnetic Coupling Mechanism with Different Primary and Secondary Coils for Maximum Output Power

Zhongyu Dai<sup>1</sup> · Wenxi Peng<sup>2</sup> · Yake Tang<sup>3</sup> · Haoran Xu<sup>4</sup> · Huihui Wang<sup>1</sup> · Yanhu Zhai<sup>1</sup> ·

Ming Xue<sup>1</sup> · Xian Zhang<sup>1,\*</sup>

---

## Abstract

---

Output power is an important performance metric related to static or quasi-static wireless power transfer (WPT). As an important component of WPT, the electrical parameters of a magnetic coupling mechanism (MCM) are directly related to its output characteristics. Notably, an optimal WPT design is largely based on MCMs using the same primary and secondary coils. However, in some scenarios involving limited space, the physical structure and electrical parameters of the coils cannot be kept completely consistent. Based on the influence of physical parameters on coupling performance and system characteristics, an optimal design method for MCMs using different primary and secondary coils to ensure maximum output power is proposed. The best receiving coil within a limited space that achieves maximum power at a specific location was selected. Experiments were conducted, with the corresponding results verifying the correctness of theoretical and simulation analyses, as well as the effectiveness of the proposed method.

**Key Words:** Coils, Magnetic Coupling Mechanism (MCM), Output Power, Wireless Power Transfer (WPT).

---

## I. INTRODUCTION

The continuous consumption of fossil fuels has made environmental problems, such as global warming, increasingly prominent. To address these circumstances, replacing petrol vehicles with electric vehicles (EVs) has become a strategic policy adopted by many countries [1–4]. Driven by the promotion of policies and incentives, the number of EVs has sharply increased. However, the widespread applications of EVs require proper solutions to their charging prob-

lems. Charging stations are the most common power replenishment equipment for EVs. However, manual operations are required in the charging process, posing risks pertaining to poor contact and electric shock on rainy days, among others [5, 6].

Wireless power transfer (WPT) offers a new solution for charging EVs [7, 8]. In WPT, the electromagnetic field is used as the medium for non-contact power transmission, thus eliminating safety issues such as sparks and electric shock. Combined with intelligent identification and control, manual operation during EV

---

Manuscript received August 13, 2023 ; Revised November 12, 2023 ; Accepted December 08, 2023. (ID No. 20230813-143J)

<sup>1</sup>State Key Laboratory of Reliability and Intelligence of Electrical Equipment, Key Laboratory of Electromagnetic Field and Electrical Apparatus Reliability of Hebei Province, Hebei University of Technology, Tianjin, China.

<sup>2</sup>Ultra High Voltage Branch, State Grid Sichuan Electric Power Company, Xichang, China.

<sup>3</sup>Economic and Technological Research Institute, State Grid Henan Electric Power Company, Zhengzhou, China.

<sup>4</sup>College of Information Science and Technology, Donghua University, Shanghai, China.

\*Corresponding Author: Xian Zhang (e-mail: zhangxian@hebut.edu.cn)

---

This is an Open-Access article distributed under the terms of the Creative Commons Attribution Non-Commercial License (<http://creativecommons.org/licenses/by-nc/4.0>) which permits unrestricted non-commercial use, distribution, and reproduction in any medium, provided the original work is properly cited.

© Copyright The Korean Institute of Electromagnetic Engineering and Science.

charging can be entirely eliminated [9, 10] and completely unmanned operations can be achieved. The modular structure of WPT allows for embedded installations that do not require additional land, which is extremely beneficial for urban planning. WPT offers numerous advantages in the field of EV charging and, therefore, has received increasing attention in recent years [11, 12].

Extensive research and exploration has been conducted on WPT for EVs, mainly with regard to the converter and magnetic coupling mechanism (MCM) [13–15]. Converter technology is relatively mature, with a general efficiency higher than 95% or even 98% [16, 17]. The design of MCM can be divided into two parts—the compensation topology and the coil structure [18, 19]. The three most common forms of compensation topologies are series and parallel compensation, which are the basic compensation topologies [20, 21], and LCC compensation, which is representative of a new compensation topology for meeting specific performance demands [14, 22]. Furthermore, a unipolar Q-type coil is the most widely used structure prevalent in MCMs [23, 24]. However, to meet the high power requirements at close distance for EVs, the use of DD-type coil has been proposed [25, 26], since it comprises two-directional magnetic fields on one side, due to which it is also known as the bipolar coil.

In published research on WPT for EV charging, the optimization of transmission performance and structural parameters has usually been based on the identical structure of the MCM, which uses the same primary and secondary coils. However, in practical applications, EV wireless charging can be significantly affected by the characteristics of WPT and the application environment. For instance:

- 1) Placing the transmitter on the ground in EV wireless charging makes it easy to achieve a unified design, but the volume of the EV receiver may be limited.
- 2) The ground clearance of different EVs varies. Therefore, diverse kinds of EVs need to be optimized and designed under various transmission distances to achieve better performance.
- 3) Different batteries have varying characteristics. Therefore, to determine the optimal receiver, EV wireless charging needs to be adjusted according to the properties of the batteries.

Compared to fuel-based vehicles, EVs are at a disadvantage with regard to their power replenishment time. Addressing this issue would require greater output power from WPT to shorten the charging time [4, 11, 27]. Therefore, to build a unified transmitter, a targeted design should be developed for receivers of different EVs to achieve maximum power. The traditional optimal method for achieving maximum output power using the same coils is no longer applicable. Therefore, in this study, a design method for the MCM that employs heterogeneous primary and secondary coils is proposed. The size of the receiving coil, the transmission distance, and the load differences are com-

prehensively examined to achieve maximum output power at a fixed distance within a limited design space.

## II. THEORETICAL ANALYSIS

### 1. Transmission Performance of WPT

In an LC resonant circuit, the frequency  $f$  of voltage and current are not affected by the ideal resonant frequency  $f_0 = 1/\sqrt{LC}$ , which always remains the same as the frequency  $f_{source}$  of the source. The difference in frequency  $\Delta f = |f_0 - f_{source}|$  between the LC and the source only affects the equivalent impedance  $X_{LC} = 2\pi f_{source}L - 1/2\pi f_{source}C$ . In WPT, LC resonance, which is composed of coil inductance and compensation capacitance, exhibits the same characteristics. The simplified equivalent circuit for WPT using a series-series (SS) compensation topology is shown in Fig. 1. Notably,  $R_t = R_s + R_{l1}$  and  $R_r = R_l + R_{l2}$  refer to the total resistance of the primary and secondary sides,  $X_t = \omega L_1 - 1/\omega C_1$  and  $X_r = \omega L_2 - 1/\omega C_2$  denote the total reactance, and  $X_M = \omega M$  is the mutual inductance reactance. Notably, Kirchhoff's voltage law proposes the following equation:

$$\begin{bmatrix} \dot{U}_s \\ 0 \end{bmatrix} = \begin{bmatrix} R_t + jX_t & -jX_M \\ -jX_M & R_r + jX_r \end{bmatrix} \begin{bmatrix} \dot{I}_t \\ \dot{I}_r \end{bmatrix}, \quad (1)$$

where current  $\dot{I}_t$  and  $\dot{I}_r$  of the primary and second sides, respectively, can be formulated as follows:

$$\begin{cases} \dot{I}_t = \frac{[AR_r + BX_r + j(AX_r - BR_r)]\dot{U}_s}{A^2 + B^2} \\ \dot{I}_r = \frac{(jA + B)X_M\dot{U}_s}{A^2 + B^2} \end{cases} \quad (2)$$

where  $A = R_tR_r + X_M^2 - X_tX_r$ ,  $B = R_tX_r + R_rX_t$ .

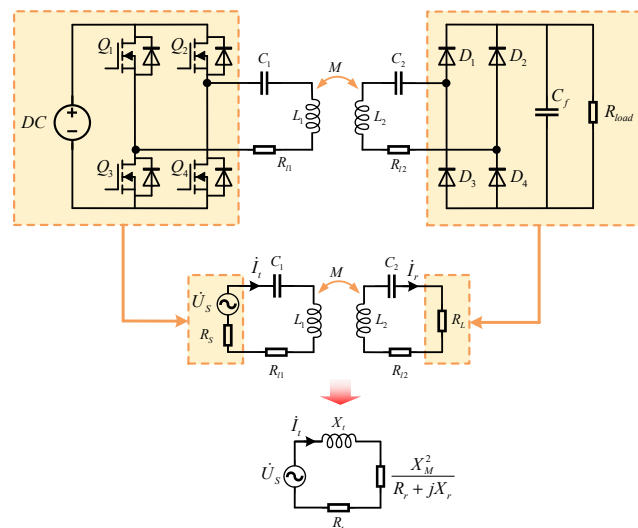


Fig. 1. Equivalent circuit of WPT with SS compensation topology.

Furthermore, the input power  $P_{in}$ , output power  $P_{out}$ , and transmission efficiency  $\eta$  can be expressed as follows:

$$P_{in} = \text{Re} [\dot{U}_S \dot{I}_t^*] = \frac{(AR_r + BX_r)U_S^2}{A^2 + B^2} \quad (3)$$

$$P_{out} = I_r^2 R_L = \frac{X_M^2 U_S^2 R_L}{A^2 + B^2} \quad (4)$$

$$\eta = \frac{P_{out}}{P_{in}} = \frac{X_M^2 R_L}{AR_r + BX_r} \quad (5)$$

where  $U_S$  and  $I_r$  are the modulus values of  $\dot{U}_S$  and  $\dot{I}_r$ .

Based on Eq. (5), the variation in transmission performance with regard to mutual inductance was obtained, as shown in Fig. 2. It is noted that the larger the mutual inductance reactance  $X_M$ , the higher the transmission efficiency  $\eta$ . In other words, an increasing mutual inductance  $M$  or resonant frequency  $f$  can improve  $\eta$ . Furthermore, when output power  $P_{out}$  attains its maximum value,  $X_M$  must satisfy the following equation:

$$X_M^2 = \sqrt{(R_t^2 + X_t^2)(R_r^2 + X_r^2)} = |Z_t||Z_r|, \quad (6)$$

where  $|Z_t| = \sqrt{R_t^2 + X_t^2}$  and  $|Z_r| = \sqrt{R_r^2 + X_r^2}$  are the amplitudes of the primary and secondary impedances.

Moreover, for WPT with determined physical parameters, a unique value of mutual inductance  $M$  that maximizes the output power is usually considered. The maximum output is

$$P_{out-max} = \frac{U_S^2 R_L}{2|Z_t||Z_r| + 2(R_t R_r - X_t X_r)} \quad (7)$$

When the primary and secondary sides of the MCM have the same resonant frequency, which is the same as that of the source, the ideal resonant state is achieved,  $X_t = X_r = 0$ . Therefore, Eqs. (6) and (7) can be simplified as follows:

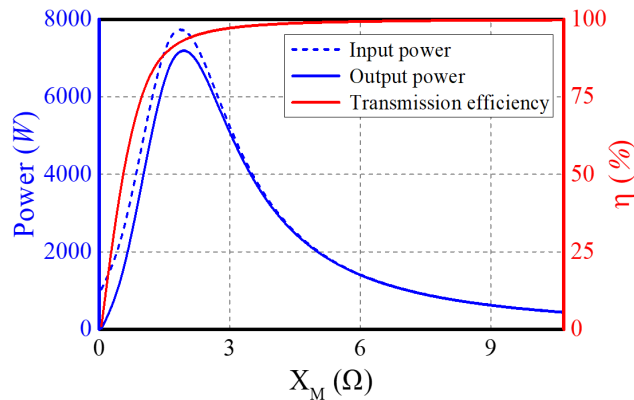


Fig. 2. Relationship between transmission performance and mutual inductance.

$$\begin{cases} X_M^2 = R_t R_r \\ P_{out-max} = \frac{U_S^2 R_L}{4R_t R_r} \end{cases} \quad (8)$$

## 2. Maximum Output Power of the MCM

For an MCM characterized by different primary and secondary coils, the most significant electrical parameter characteristics are the unequal inductances  $L_1$  and  $L_2$ . To meet resonance conditions, it may be assumed that the compensating capacitances and inductances satisfy  $L_1 C_1 = L_2 C_2$ . On determining the structural parameters of the transmitting coil and the resonance frequency  $f$ , Eqs. (6) and (7) indicate that the maximum output power is restricted by the secondary impedance  $X_r$  and the mutual inductance reactance  $X_M$ .

Notably, when the frequency  $f_{source}$  of the source is equal to the ideal resonant frequency  $f_0$ ,  $X_t = X_r = 0$  and  $Z_t = R_t$ ,  $Z_r = R_r$ . Fig. 3 shows the impact of mutual inductance reactance  $X_M$  and receiver resistance  $R_r$  on the performance of equivalent circuit, where  $R_r$  is positively correlated and  $X_M$  is negatively correlated with input power  $P_{in}$ . Furthermore, when either  $R_r$  or  $X_M$  is kept constant, the output power  $P_{out}$  will initially increase and then decrease with an increase  $R_r$  or  $X_M$ . As for the transmission efficiency  $\eta$ , as shown in Fig. 3(c), it increases continuously with an increase in  $X_M$  or a decrease in  $R_r$ , indicating an opposite trend as that of  $P_{in}$ .

If the frequency  $f_{source}$  of the source is not equal to the ideal resonant frequency  $f_0$ ,  $X_t/L_1 = X_r/L_2 \neq 0$ . Assuming  $f_{source} = f_0 + \Delta f$ , the receiver impedance  $Z_r$  cannot be considered purely resistive. Fig. 4 depicts the impact of mutual inductance reactance  $X_M$  and receiver resistance  $R_r$  on the performance of WPT under non-ideal resonant conditions. Notably, the variation trend of the output power  $P_{out}$  and transmission efficiency  $\eta$  is the same as that shown in Fig. 3(b) and 3(c). However, the maximum output power  $P_{out-max}$  is reduced. This indicates that the power difference in  $P_{out-max}$  is related to the frequency difference  $\Delta f$ —the greater the  $\Delta f$ , the greater the reduction in  $P_{out-max}$ . Furthermore, the input power  $P_{in}$  in Fig. 4(a) is different from that in Fig. 3(a). This variation is the same as that of  $P_{out}$  under non-ideal resonant conditions—increasing initially to then decrease with an increase in  $X_M$  or  $R_r$ .

Based on the output power estimations shown in Figs. 3 and 4, a unique mutual inductance reactance  $X_M$  is observed, which achieves the maximum output power  $P_{out-max}$  for any receiver impedance  $Z_r$ , thus satisfying Eq. (6). Furthermore,  $X_M = \omega M$  is influenced by mutual inductance  $M$  and angular frequency  $\omega$ . The primary and secondary impedances— $Z_t = R_t + j\omega L_t + 1/j\omega C_t$  and  $Z_r = R_r + j\omega L_r + 1/j\omega C_r$ —are influenced by coil resistances  $R_{AC}$ , self-inductances  $L$ , and angular frequency  $\omega$ . Moreover,  $M$ ,  $R_{AC}$ , and  $L$  are found to be closely related to the physical parameters and the relative spatial

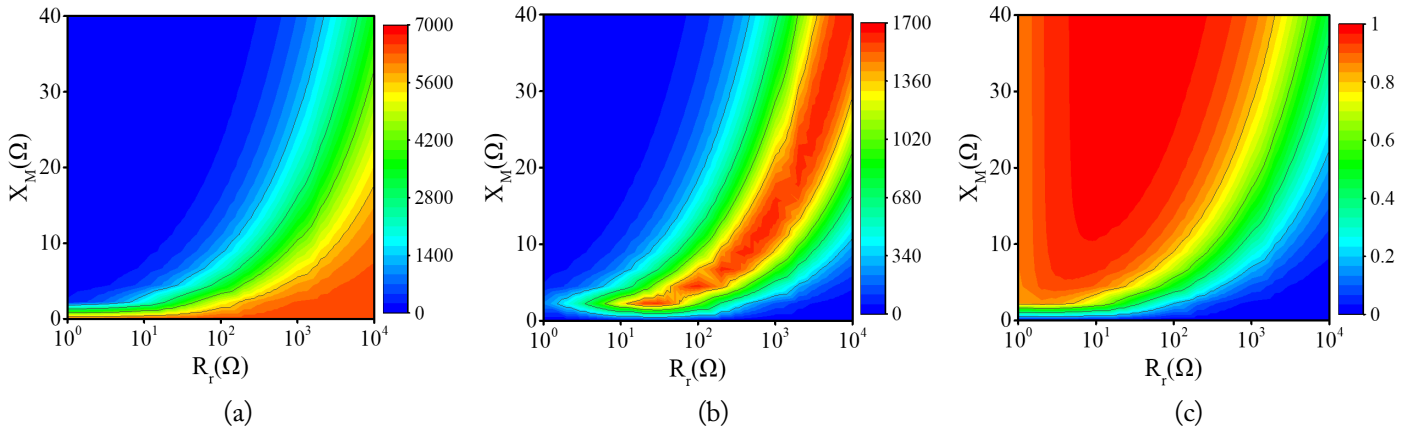


Fig. 3. Influence of mutual inductance reactance  $X_M$  and receiver resistance  $R_r$  on performance under ideal resonant conditions: (a) input power  $P_{in}$ , (b) output power  $P_{out}$ , and (c) transmission efficiency  $\eta$ .

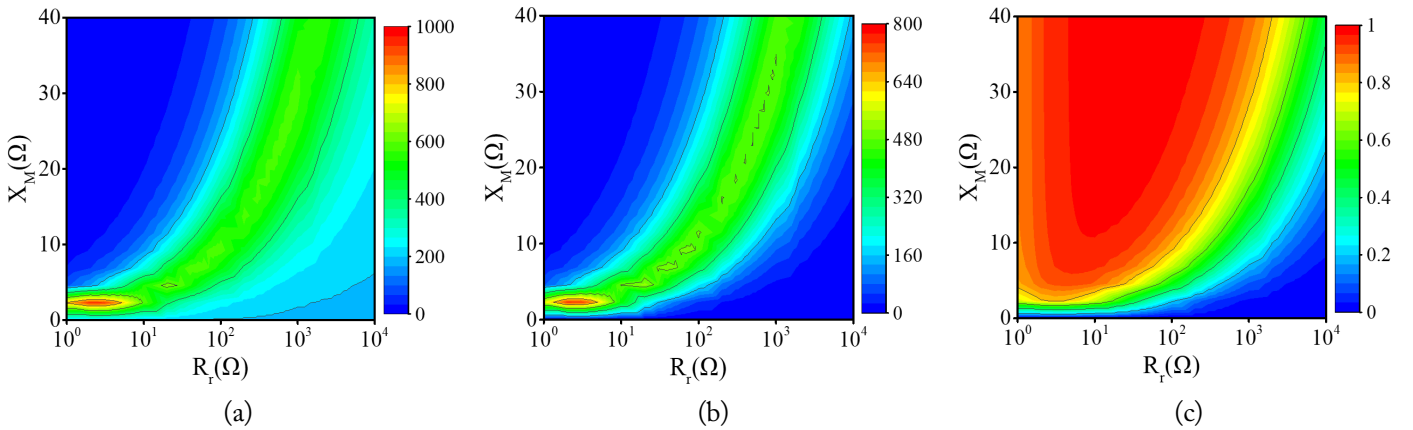


Fig. 4. Influence of mutual inductance reactance  $X_M$  and receiver resistance  $R_r$  on performance under non-ideal resonant conditions: (a) input power  $P_{in}$ , (b) output power  $P_{out}$ , and (c) transmission efficiency  $\eta$ .

position of the coils. Notably, during static WPT, the relative spatial position of the coils usually remains constant. This paper takes advantage of the effects of the physical parameters of coils on their electrical characteristics to optimize their structure and maximize their output power.

### III. ELECTRICAL PARAMETERS OF THE MCM

For the MCMs used for EVs, electromagnetic shielding is usually implemented to reduce electromagnetic leakage and improve transmission performance, as shown in Fig. 5(a). Notably, the influence of electromagnetic shielding on the electrical parameters of coils does not change the impact of its physical parameters on self-inductance or mutual inductance [28, 29]. In other words, the difference in electrical parameters between two typical MCMs, as shown in Fig. 5, is mainly reflected in the relative magnetic permeability  $\mu$ . To simplify the analysis process, this study considers an MCM without electromagnetic shielding, as shown in Fig. 5(b), as an example.

To achieve maximum output power within a limited design space, appropriate parameters and structure of the MCM need to

be selected and optimized based on the application scenario. Therefore, the mutual inductance and impedance were adjusted to satisfy Eq. (6). For a typical MCM without electromagnetic shielding, as depicted in Fig. 6, the optimization of its physical parameters involves (i) both its transmitting and receiving coils, and (ii) either the transmitting or receiving coil. In the case of EV wireless charging, the transmitting coil can be flexibly designed, but the receiving coil is limited by the size of the EV chassis, which indi-

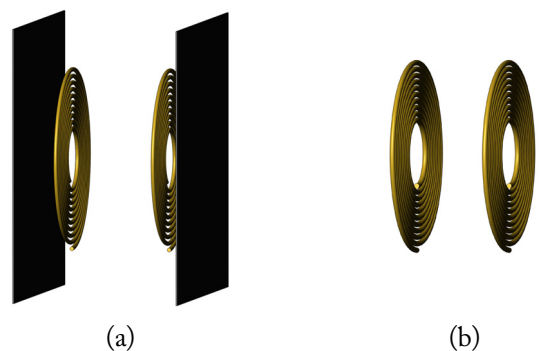


Fig. 5. A typical MCM with two coils: (a) with electromagnetic shielding and (b) without electromagnetic shielding.

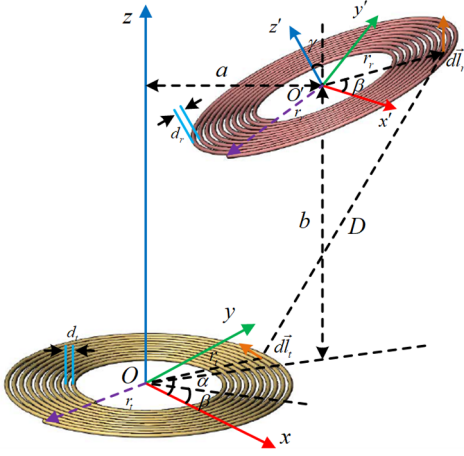


Fig. 6. A typical MCM without electromagnetic shielding.

icates that Situation (ii) applies in this particular context. Therefore, the current paper selected this situation as an example for optimizing the MCM. Subsequently, the transmitting coil and the relative spatial position were fixed, while the receiving coil was designed within a limited space to obtain the maximum output power.

### 1. Mutual Inductance

Mutual inductance refers to the ratio of the magnetic flux linking any coil to the current-producing magnetic flux in the other coil. For two parallel single-turn circular coils [30], the mutual inductance can be expressed as follows:

$$M_{ij}(RC_i, RC_j, D_{i,j}) = \frac{2\mu_0}{\alpha_{ij}} \sqrt{RC_i RC_j}, \quad (9)$$

where  $\alpha_{ij} = 2\sqrt{RC_i RC_j / [(RC_i + RC_j)^2 + D_{ij}^2]}$ ,  $\mu_0$  is the permeability of vacuum,  $RC_i$  and  $RC_j$  are the radii of the two single-turn coils, and  $D_{ij}$  is the center-to-center distance of the two single coils. Furthermore,  $P(\alpha_{ij})$  and  $Q(\alpha_{ij})$  are the complete elliptic integrals of the first and second kinds, respectively.

Notably, a multi-turn coil can be considered equivalent to some single-turn coils with a continuously varying radius. Furthermore, since the coil radius  $RC$  is usually much larger than the wire radius  $r$ , the effect of  $r$  can be ignored. Therefore, the equivalent radius of the  $i^{th}$  single-turn coil from the center can be formulated as  $RC_i \approx RC_0 + (i - 1)d$ , where  $d$  is the pitch. Notably, all single-turn coils have the same center. Furthermore, the distance  $D_{t,r}$  between the center of the transmitting coil and the receiving coil also remains constant. Assuming that the turns of the transmitting and receiving coils are  $N_t$  and  $N_r$ , the mutual inductance of MCM can be represented as follows:

$$M = \sum_{t=1}^{N_t} \sum_{r=1}^{N_r} M_{t,r}(RC_t, RC_r, D_{t,r}). \quad (10)$$

Mutual inductance is influenced by multiple factors, which can be divided into two categories—the physical parameters of the coils, including the pitch  $d_t$ ,  $d_r$ , turns  $N_t$ ,  $N_r$ , outer radii  $RC_t$ , and  $RC_r$ , and the relative spatial position parameters  $D_{t,r}$ , also known as spatial parameters of the MCM, including the vertical spacing  $b$ , horizontal offset  $a$ , and tilt angle  $\gamma$ . In static WPT, spatial parameters, usually regarded as known parameters in an optimal design, can be obtained through measurement and prediction.

To carry out an in-depth emamination of the influence of physical parameters on mutual inductance, a simulation model was employed in this study. According to the symmetry characteristics and magnetic field distribution of the MCMs, the transmitting and receiving coils have the same effect on mutual inductance. Therefore, in the simulation, only the parameters of the receiving coil were changed. Furthermore, to eliminate the influence of specific parameter values, the physical and electrical parameters were synchronously normalized, the function for which can be defined as follows:

$$\chi = \frac{\zeta}{\zeta_{av}}, \quad (11)$$

where  $\zeta_{av}$  represents the mean value of each parameter within the change range.

The outer radius  $RC_r$ , turns  $N_r$ , pitch  $d_r$ , and the mutual inductance  $M$  were synchronously normalized based on Eq. (11), the results of which are shown in Fig. 7. The slopes of the curves in Fig. 7 represent the strength of the influence of physical parameters on mutual inductance. A positive slope indicates an active impact, while slopes less than 0 indicate a negative correlation. In other words, the greater the absolute value of the slope, the more significant the effect. According to the variations of the curves observed in Fig. 7, it is evident that  $RC_r$  and  $N_r$  are positively correlated with  $M$ , while  $d_r$  is negatively correlated. Furthermore, the slopes corresponding to  $RC_r$  and  $d_r$  are approximately constant, indicating a linear correlation between  $RC_r$ ,  $d_r$ , and  $M$ . It is further observed that as  $N_r$  increases, the rate of change of  $M$  decreases continuously. This may be attributed to the fact that when  $N_r$  increases while  $RC_r$  and  $d_r$  are constant, the increased  $RC$  gradually starts to decline, as a result of which the influence of  $N_r$  on  $M$  will continue to weaken.

From Fig. 7, it is evident that changing the transmitting coil does not affect the impact of the receiving coil on mutual inductance. Therefore, when a single-sided coil is optimized, the parameters of the other side can be considered known. Overall, the influence of the physical parameters of a single-sided coil on mutual inductance  $M$  can be expressed as

$$M = x_1(RC_r, N_r, d_r). \quad (12)$$

## 2. Self-Inductive

Mutual inductance is defined as the ratio of the magnetic flux linking one coil to the current-producing magnetic flux in the same coil [31, 32]. Its corresponding equation can be presented as:

$$L(RC_i, r_i) = \mu_0 RC_i \left[ \ln \left( \frac{8RC_i}{r_i} \right) - 2 \right], \quad (13)$$

where,  $RC_i$  is the radius of the single-turn coil and  $r_i$  is the radius of the wire.

All equivalent single-turn coils have the same center— $D_{t,r} = 0$ . The self-inductance of a coil with  $N_r$  turns can be formulated as:

$$L = \sum_{r=1}^N L(RC_r, r) + \sum_{t=1}^N \sum_{r=t+1}^N M_{t,r}(RC_t, RC_r, D_{t,r} = 0). \quad (14)$$

According to Eq. (14), self-inductance is mainly influenced by its own turns  $N_r$ , radius  $RC_r$ , pitch distance  $d_r$ , and wire radius  $r_r$ . Therefore, during coil design,  $r_r$  is usually determined based on electrical parameters, such as current and voltage. Only  $N_r$ ,  $RC_r$ , and  $d_r$  are the optimal targets for the coil structure. The results processed using Eq. (11) are presented in Fig. 8, which shows that the changes in the curves are similar to those shown in Fig. 7. The radius  $RC_r$  and turns  $N_r$  are positively correlated with self-inductance  $L_r$ , while the pitch  $d_r$  is

negatively correlated with the same. Furthermore,  $RC_r$  and  $d_r$  are linearly correlated with  $L_r$ . Notably,  $RC_r$  and  $N_r$  correspond to a larger curve slope, meaning that these parameters have a more obvious influence on  $L_r$ .

Therefore, the self-inductance of a coil is constrained only by its own physical parameters, which can be expressed as:

$$L = x_2(RC_r, N_r, d_r). \quad (15)$$

## 3. Resistance

The AC losses of an MCM comprise ohmic losses and radiation losses [7]. Ohmic losses dominate in the low-frequency range, while radiation losses become prevalent at high frequencies. For EV wireless charging, the resonant frequency generally remains between 80 kHz and 100 kHz, thus falling in the low-frequency range. Therefore, in this case, radiation losses can be neglected. As a result, only ohmic resistance was considered in this experiment, which can be expressed as follows:

$$R_{AC} = \sqrt{\frac{\mu_0 \omega}{2\sigma}} \frac{l}{4\pi r} = \sqrt{\frac{\mu_0 \omega}{2\sigma}} \frac{2R - (N-1)d}{8\pi r} N, \quad (16)$$

refers to the pitch,  $\omega$  denotes angular frequency, and  $\sigma$  indicates conductivity.

According to Eq (16), the AC resistance  $R_{AC}$  is influenced by the operating parameters (angular frequency  $\omega$ ), wire material (conductivity  $\sigma$ , wire radius  $r$ ), and structure parameters (radius

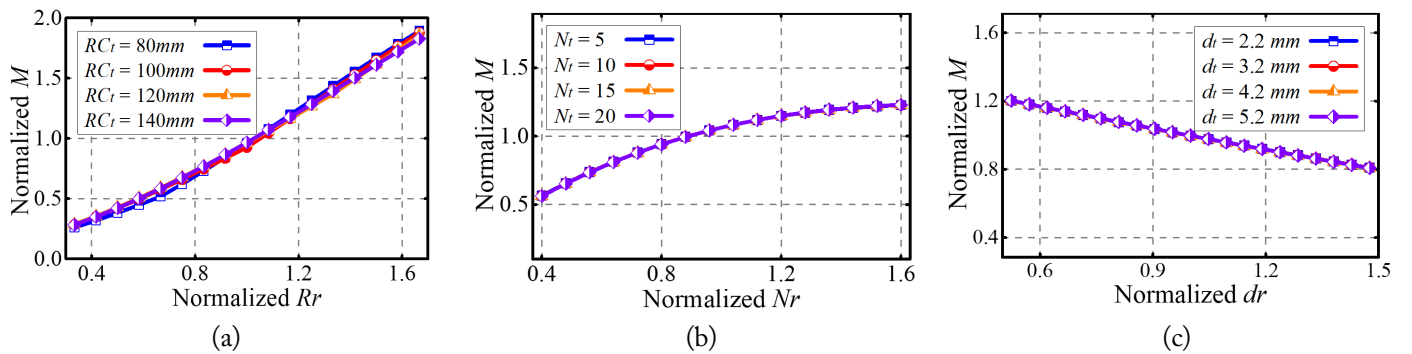


Fig. 7. Influence of physical parameters on mutual inductance: (a) outer radius, (b) turns, and (c) pitch.

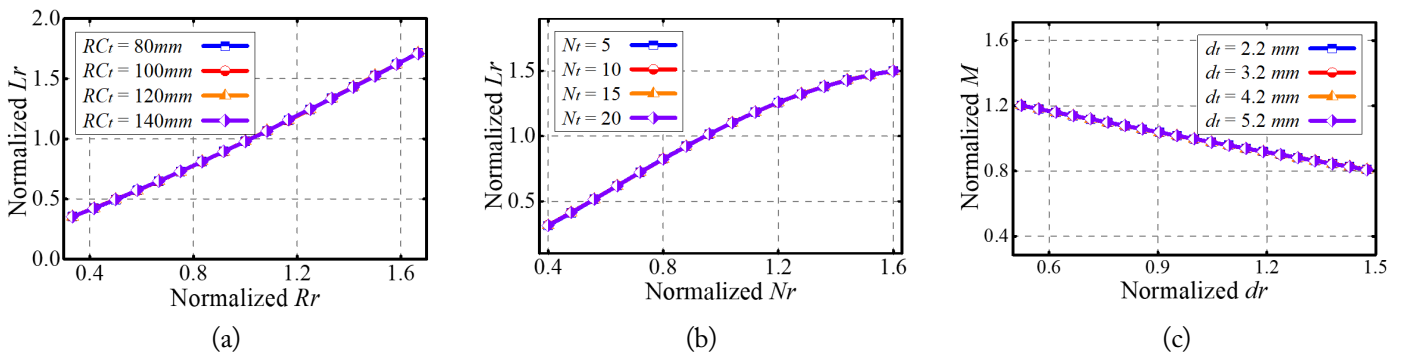


Fig. 8. Influence of physical parameters on self-inductance: (a) outer radius, (b) turns, and (c) pitch.

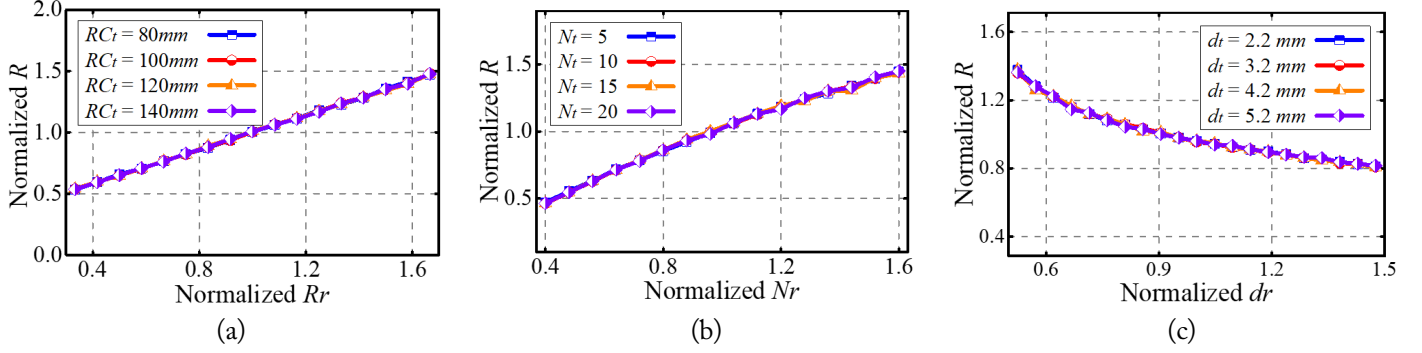


Fig. 9. Influence of physical parameters on AC resistance: (a) outer radius, (b) turns, and (c) pitch.

$RC$ , turns  $N$ , pitch  $d$ ). Therefore, the proposed design focused on structure parameters. The impact of physical parameters on AC resistance  $R_{AC}$  is demonstrated in Fig. 9.

Notably, the curves shown in Fig. 9 were also normalized. The influence of physical parameters on AC resistance  $R_{AC}$  is consistent with the overall trend shown in Figs. 7 and 8. The outer radius  $RC_r$  and turns  $N_r$  are linearly positively correlated with  $R_{AC}$ , while pitch  $d_r$  is negatively correlated. Essentially, it is observed that an increase in  $RC_r$  and  $N$  will lengthen the total length of wire  $l$ , while the increase in  $d_r$  will shorten it. Furthermore, Litz wire is usually used in WPT, as it can effectively mitigate the skin effect and proximity effect. There exists a linear relationship between physical parameters and  $R_{AC}$ . It is only when  $d_r$  is very small that it will exhibit a reduced skin effect. In other words,  $R_{AC}$  gradually decreases and eventually stabilizes with an increases of  $d_r$ .

AC resistance  $R_{AC}$  is also restricted by radius  $RC_r$ , turns  $N_r$ , and pitch  $d_r$ , which can be expressed as follows:

$$R_{AC} = x_3(RC_r, N_r, d_r). \quad (17)$$

Overall, based on the effects of physical parameters on electrical parameters, Figs. 7–9 show that the outer radius  $RC_r$ , turns  $N_r$ , and pitch  $d_r$  have an almost similar influence on mutual inductance  $M$ , self-inductance  $L$ , and AC resistance  $R_{AC}$ .

## IV. OPTIMIZATION OF THE MCM

### 1. Influence of Resonance Frequency

Based on the theories demonstrated above, resonance frequency  $f$  is another crucial factor that affects the maximum output power  $P_{out-max}$ . Eq. (6) clearly shows that  $f$  influences  $P_{out-max}$ , primary impedance  $Z_t$ , secondary impedance  $Z_r$ , and mutual inductance reactance  $X_M$ . The impact of  $f$  and mutual inductance  $M$  on transmission performance, based on Eqs. (3)–(5), are shown in Fig. 10, where the black dashed line corresponds to the ideal resonant frequency  $f_0$ . The area to its right represents the under-compensation area, where the primary reactance  $X_t$  and secondary reactance  $X_r$  are inductive. Moreover, input power  $P_{in}$  and output power  $P_{out}$  have the same variations. When frequency  $f$  reaches close to  $f_0$ , the maximum output power  $P_{out-max}$  is achieved, while the corresponding mutual inductance  $M$  is the smallest. Furthermore, as  $f$  increases, the required  $M$  for  $P_{out-max}$  increases along with it. This is because when  $f$  deviates from  $f_0$ ,  $X_t/L_1 = X_r/L_2 \neq 0$ . This means that the larger the deviation, the larger the  $X_t$  and  $X_r$ . Since the modulus of the primary and secondary impedances  $|Z_t|$  and  $|Z_r|$  are also larger, a larger  $X_M$  was required. In addition, for the transmission efficiency  $\eta$  in Fig. 10(c), the higher the  $M$ , the higher the  $\eta$ . Therefore,  $\eta$  is also affected by  $f$ . A small  $M$  results in a

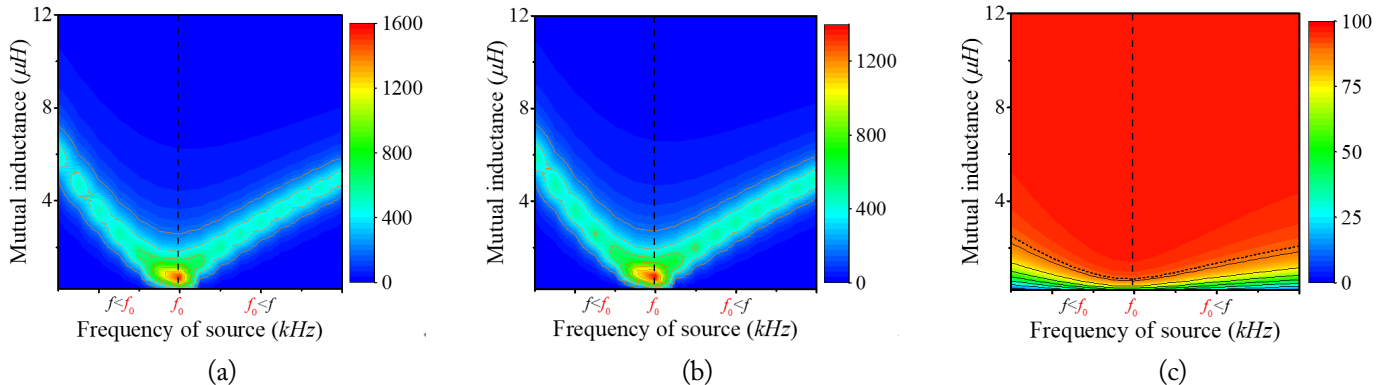


Fig. 10. The transmission performance varying with the mutual inductance and frequency: (a) input power (W), (b) output power (W), and (c) transmission efficiency (%).

higher  $f$  and lower  $\eta$ . At  $f_0$ , the required  $M$  is at its minimum. This is also why both the primary and secondary sides of an MCM should work in a resonant state as much as possible.

### 2. Design of the Receiving Coil

The design process for the receiving coil to obtain the maximum output power  $P_{out-max}$  is shown in Fig. 11. First, the wire radius  $r$ , load  $R_l$ , and resonance frequency  $f$  were determined based on the requirements of EV wireless charging. In a single-sided restricted MCM, the physical parameters of a transmitting coil and its relative spatial position are known conditions. Furthermore, self-inductance  $L_t$  and resistance  $R_{l1}$  of the transmitting coil were determined using Eqs. (15) and (17). For this purpose, the primary and secondary coils with similar or identical structures and parameters were considered the most favorable. Notably, for a restricted receiving coil, the radius  $RC_r$  should be as close as possible to that of the transmitting coil. Moreover, since the resistance of coils is usually small,  $R_{l1}$  is generally higher than the resistance of the source and the compensation capacitor. Therefore, it is included in  $Z_t$ . However, resistance  $R_{l2}$  of the receiving coil is usually ignored. Additionally, to reduce losses, the influence of the skin effect should be weakened as much as possible. The optimal pitch  $d_r$  was selected based on  $f$ . Subsequently, based on Eq. (6), the optimal impedance  $X_M$  was calculated. The outer radius  $RC_r$ , turns  $N_r$ , and pitch  $d_r$  of the receiving coil were selected using Eqs. (12), (15), and (17).

When both the primary and secondary sides of an MCM are in ideal resonance,  $X_t = X_r = 0$ ,  $Z_t = R_t$ , and  $Z_r = R_r$ . The effect of self-inductance  $L_r$  of the receiving coil can be ignored, since it only needs to satisfy Eq. (6). In such a case, the turns of the receiving coil can be calculated without accounting for Eq. (15). As shown in Fig. 4, when the resonance frequency  $f$  deviates from the ideal value—that is, when it is in non-ideal resonance—an optimal mutual inductance  $M$  is present. Therefore, the effects of the self-inductances of both the transmitting and receiving coils must be accounted for in the design process shown in Fig. 11.

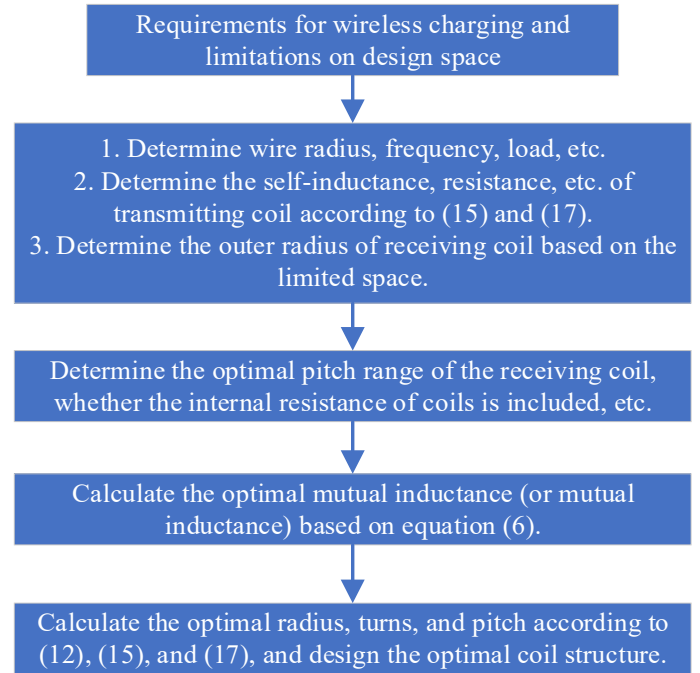
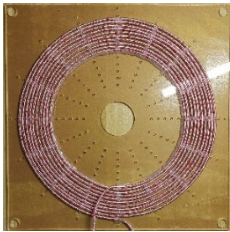
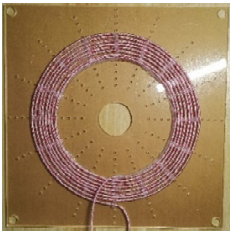
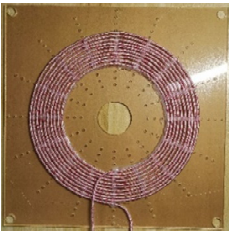
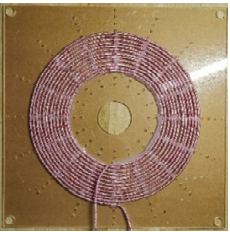


Fig. 11. Design flow of an optimal receiving coil.

## V. EXPERIMENTS

Four coils were wound with  $0.1 \text{ mm} \times 500$  Litz wire, maintaining a pitch of 5 mm. One of the coils was a transmitting coil, while the other three were receiving coils. The representative symbols and corresponding structures are listed in Table 1, while the physical and electrical parameters of the four coils are shown in Table 2. Excluding the reserved length of the wire, the total lengths of the four coils were  $250\pi$  cm,  $176\pi$  cm,  $210\pi$  cm, and  $240\pi$  cm. The ratio of wire length to AC resistance was approximately equal, consistent with the theoretical derivation in Eq. (16). Furthermore, the ratio of self-inductance to the number of turns was closely aligned with the law depicted in Fig. 8(b). Notably, the SS compensation topology was selected. Coils and corresponding compensation capacitors together formed the

Table 1. Symbols and their means and structures

Symbol	TC	RC1	RC2	RC3
Means	Transmitting coil	Receiving coil 1	Receiving coil 1	Receiving coil 3
Structure				
Wire length of coil (cm)	$250\pi$	$176\pi$	$210\pi$	$240\pi$
Optimal transmission distance (cm)	—	25	27	28



transmitter and the different receivers, ultimately generating different MCMs. The representative symbols and meanings of the transmitter, receivers, and MCMs are presented in Table 3.

The resonant frequency was selected as 85 kHz. A vector analyzer (TH2826) was employed to perform the impedance characteristics. The sweep frequency range was 50 kHz–150 kHz. Notably, compensation capacitances of the transmitter and receivers were adjusted to meet the reactance  $X$  of 0 in frequency  $f = 85$  kHz. Fig. 12 traces the variations in  $X$  and resistance  $R$  with  $f$ . It is evident that  $X$  increases continuously with an increase in  $f$ , changing from negative (capacitive) to positive (inductive). Notably, compensation capacitor banks are composed of standard capacitors (with certain errors). Table 2 presents the actual compensation capacitances calculated. Due to the parasitic capacitances of the coils, the actual compensation capacitances were slightly lower than those calculated based on resonance. Furthermore, the resistances of the transmitter and receivers were approximately the sum of those of the coils and the corresponding capacitors.

This study constructed three MCMs, as shown in Table 3. Fig. 13 presents the variation in mutual inductance  $M$  with transmission distance  $D$  when the transmitting and receiving coils face each other. It is observed that as  $D$  increases,  $M$  continues to decrease—first fast and then slow. Furthermore, the more turns the receiving coil has, the greater the  $M$  of the MCM that it forms. This result is consistent with the theoretical analysis, thus verifying that in a limited space (that is, the

radius of coils remains unchanged), the adjustment of turns can ensure that the same  $M$  at different  $D$ .

Under ideal resonant conditions, the load  $R_L$  remained constant, but the transmission distances  $D$  of the MCMs changed (essentially, the change in mutual inductance  $M$  in Fig. 13). Furthermore, Fig. 14 shows the variations in output power  $P_{out}$  and transmission efficiency  $\eta$  with the transmission distance  $D$ . It is evident that the trends of all three MCMs are the same. As  $D$  increases,  $P_{out}$  increases at first and then declines.  $\eta$  shows a continuous downward trend. Furthermore, the more the turns of the receiving coil, the greater the  $\eta$ . All three MCMs achieved maximum  $P_{out}$  at  $\eta$  of around 50%. However, the optimal  $D$  corresponding to the maximum  $P_{out}$  was different—25 cm, 27 cm, and 28 cm for the three MCMs.

To achieve maximum output power  $P_{out}$ , Eq. (6) had to be met. At ideal resonance frequency  $f_0$ , the primary impedance  $Z_t$  refers to the sum of the resistances of the coil and compensation capacitor, which showed almost no change. Meanwhile, the secondary impedance  $Z_r$  includes the resistances of the coil, compensation capacitor, and load. Usually, the resistance  $R_L$  of a load is significantly greater than that of the receiver, with  $Z_r$  being approximately equal to  $R_L$ . Notably, the transmission distances  $D$  corresponding to the three images are found to be 25 cm, 27 cm, and 28 cm, representing the optimal  $D$  corresponding to the different MCMs. The three curves in Fig. 15 correspond to the  $P_{out}$  and  $\eta$  of the three MCMs. Their variations are almost identical to Fig. 14. As  $R_L$  increases,  $P_{out}$  increases at first and then decreases, while  $\eta$  shows a continuous decrease

Table 2. Physical and electrical parameters of MCM

	TC	RC1	RC2	RC3
Radius (mm)	150	130	130	130
Turns	10	8	10	12
Pitch (mm)	5	5	5	5
Self-inductive ( $\mu\text{H}$ )	38.55	22.61	30.27	37.52
Compensation capacitor (nF)	88.68	153.86	113.88	92.71

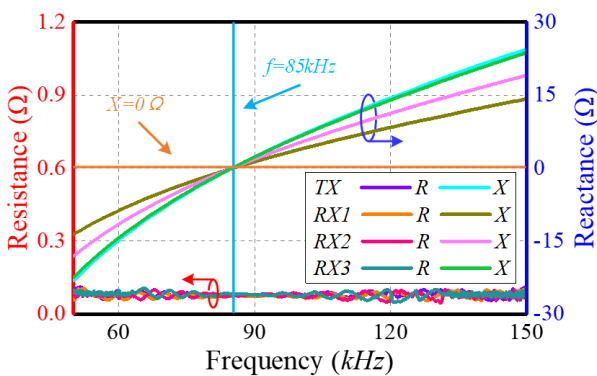


Fig. 12. The impedance and resistance varying with frequency.

Table 3. Symbols and their means

Symbol	Means
$TX, RX1, RX2, RX3$	TC, RC1, RC2, RC3 and their corresponding compensation capacitances
MCM1	MCM composed of TX and RX1
MCM2	MCM composed of TX and RX2
MCM3	MCM composed of TX and RX3

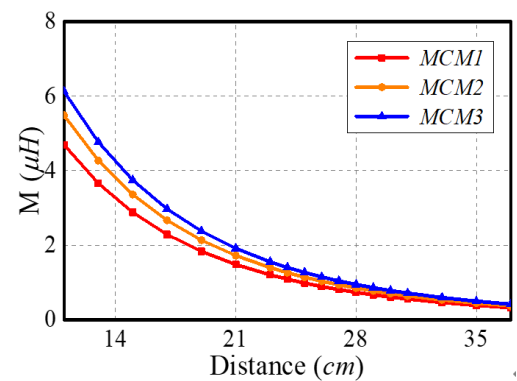


Fig. 13. Mutual inductance varying with transmission distance.

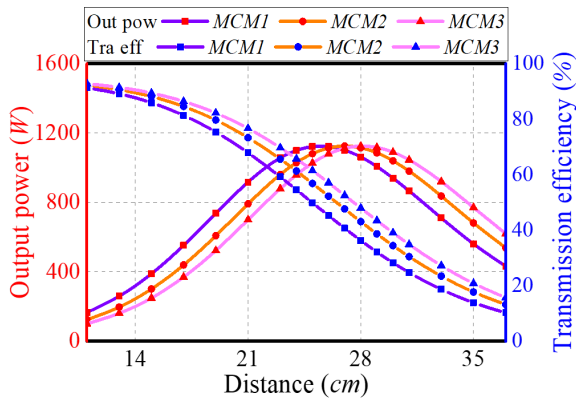


Fig. 14. Variations in output power and transmission efficiency with transmission distance.

ing trend. Furthermore, the more the turns of the receiving coil, the greater the corresponding optimal  $R_L$ . Also, the farther the  $D$ , the smaller the corresponding optimal  $R_L$ . Moreover, the three pictures shown in Fig. 15 indicate that the MCMs corresponding to the maximum  $P_{out}$  are  $MCM1$ ,  $MCM2$ , and  $MCM3$ . This implies that the change in  $R_L$  does not affect the optimal  $D$  corresponding to the different MCMs.

Under non-ideal resonance conditions, frequency  $f$  tends to have an impact on mutual inductance reactance  $X_M$ , primary

impedance  $Z_t$  and secondary impedance  $Z_r$ . In theory, as long as Eq. (6) is satisfied, WPT can extract the maximum output power  $P_{out}$ . Fig. 16 presents the variation in output power  $P_{out}$  and transmission efficiency  $\eta$  with  $f$  when the mutual inductance  $M$  and load  $R_L$  are constant. Notably, the transmission distances  $D$  corresponding to three images remains 25 cm, 27 cm, and 28 cm. However, as  $f$  increases,  $P_{out}$  and  $\eta$  first show an increasing trend that ultimately becomes a decreasing trend. The maximum values are achieved around the ideal resonant frequency  $f = f_0$ . However, the rate of change in  $P_{out}$  is considerably higher than  $\eta$ . Notably, similar to the influence of  $R_L$  on the maximum  $P_{out}$ ,  $f$  does not influence the optimal  $D$  corresponding to the different MCMs.

In obtaining the above experimental results using different MCMs, the transmitting coil remained the same. The outer radiuses of the receiving coils were also the same. Furthermore, even when the transmission distance  $D$ , load  $R_L$ , and frequency  $f$  changed, there was always an optimal MCM that was able to obtain the maximum output power  $P_{out-max}$ . The only variable for this optimal MCM was the turns  $N_r$  of receiving coil. This result verifies the feasibility of taking recourse to the adjustment of turns to achieve maximum output power for MCMs with different primary and secondary coils at a specific position.

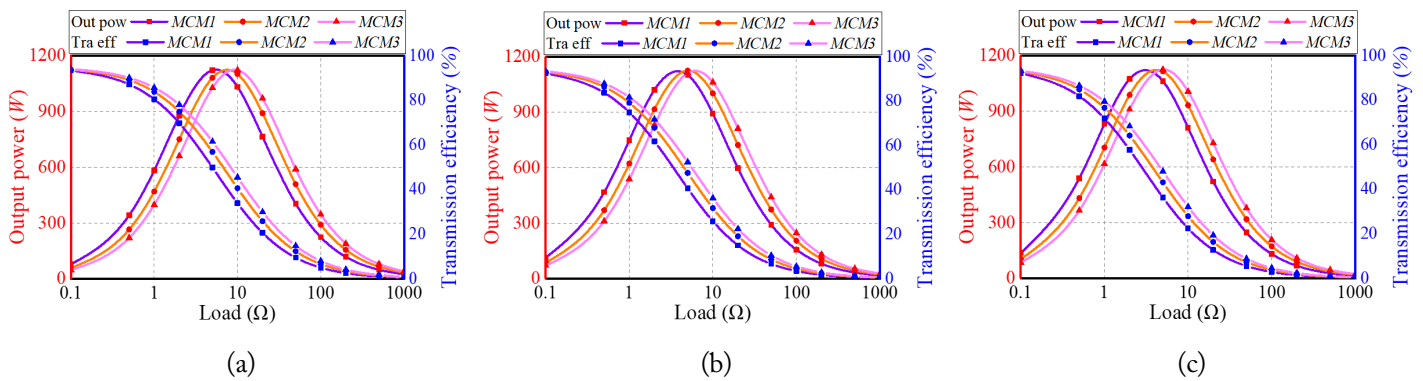


Fig. 15. Output power and transmission efficiency varying with load: (a) transmission distance is 25 cm, (b) transmission distance is 27 cm, and (c) transmission distance is 28 cm.

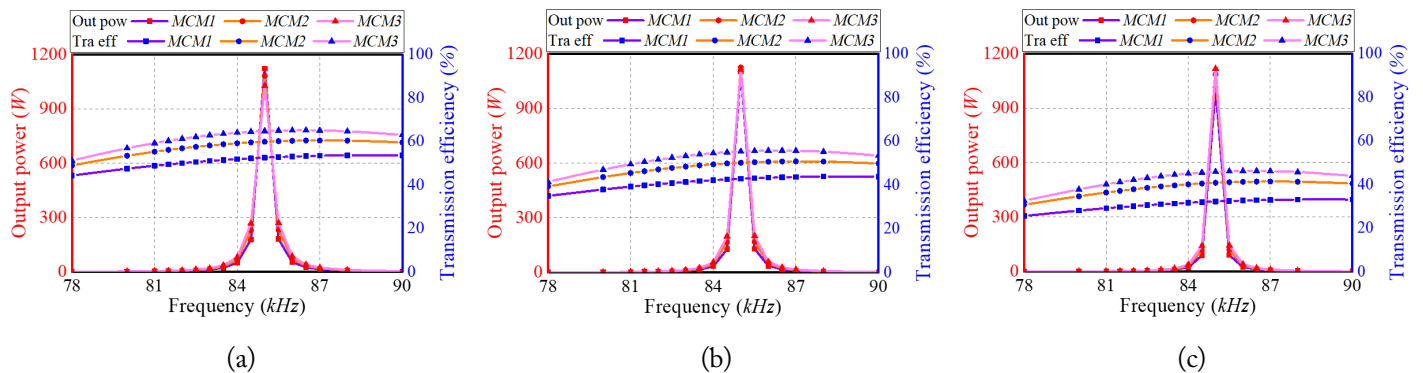


Fig. 16. Variations in output power and transmission efficiency with frequency: (a) transmission distance of 25 cm, (b) transmission distance of 27 cm, and (c) transmission distance of 28 cm.

## VI. CONCLUSION

This paper presents an optimal design method for achieving the maximum output power from MCMs using different primary and secondary coils. Detailed analyses were conducted on the impact and variation of the physical parameters on the electrical characteristics. Considering a confined space, the maximum power output for a specific transmission distance was achieved by optimizing the structural parameters of the coil. A design process for this optimal coil was also summarized. Three different MCMs were built, and relevant experiments were conducted on a 1 kW experiment platform. The differences between the best mutual inductances corresponding to the maximum output power were verified at different transmission distances, loads, and resonance frequencies. Notably, the results were found to be consistent with those of the simulations and theories, thus verifying the feasibility of the proposed optimal method.

This work was supported in part by the National Natural Science Foundation of China (Grant No. 52307008, 52122701, 51977147, and 52077153), in part by the Natural Science Foundation of Tianjin City (Grant No. 22JCZDJC00620), in part by the State Key Laboratory of Reliability and Intelligence of Electrical Equipment (Grant No. EERI\_OY2022006), and in part by the S & T Program of Hebei (Grant No. 21567605H, 215676146H, and 225676163GH).

## REFERENCES

- [1] Z. Dai and J. Wang, "A dual-frequency WPT based on multilayer self-decoupled compact coil and dual CLCL hybrid compensation topology," *IEEE Transactions on Power Electronics*, vol. 37, no. 11, pp. 13955-13965, 2022. <https://doi.org/10.1109/TPEL.2022.3183861>
- [2] K. Shi, C. Tang, H. Long, X. Lv, Z. Wang, and X. Li, "Power fluctuation suppression method for EV dynamic wireless charging system based on integrated magnetic coupler," *IEEE Transactions on Power Electronics*, vol. 37, no. 1, pp. 1118-1131, 2022. <https://doi.org/10.1109/TPEL.2021.3097504>
- [3] A. Ahmad, M. S. Alam and R. Chabaan, "A comprehensive review of wireless charging technologies for electric vehicles," *IEEE Transactions on Transportation Electrification*, vol. 4, no. 1, pp. 38-63, 2018. <https://doi.org/10.1109/TTE.2017.2771619>
- [4] Y. Zhang, Y. Wu, Z. Shen, W. Pan, H. Wang, J. Dong, X. Mao, and X. Liu, "Integration of onboard charger and wireless charging system for electric vehicles with shared coupler, compensation, and rectifier," *IEEE Transactions on Industrial Electronics*, vol. 70, no. 7, pp. 7511-7514, 2023. <https://doi.org/10.1109/TIE.2022.3204857>
- [5] O. N. Nezamuddin, C. L. Nicholas, and E. C. dos Santos, "The problem of electric vehicle charging: state-of-the-art and an innovative solution," *IEEE Transactions on Intelligent Transportation Systems*, vol. 23, no. 5, pp. 4663-4673, 2022. <https://doi.org/10.1109/TITS.2020.3048728>
- [6] D. Patil, M. K. McDonough, J. M. Miller, B. Fahimi, and P. T. Balsara, "Wireless power transfer for vehicular applications: overview and challenges," *IEEE Transactions on Transportation Electrification*, vol. 4, no. 1, pp. 3-37, 2018. <https://doi.org/10.1109/TTE.2017.2780627>
- [7] A. Kurs, A. Karalis, R. Moffatt, J. D. Joannopoulos, P. Fisher, and M. Soljacic, "Wireless power transfer via strongly coupled magnetic resonances," *Science*, vol. 317, no. 5834, pp. 83-86, 2007. <https://doi.org/10.1126/science.1143254>
- [8] W. Xiong, Q. Yu, Z. Liu, L. Zhao, Q. Zhu, and M. Su, "A detuning-repeater-based dynamic wireless charging system with quasi-constant output power and reduced inverter count," *IEEE Transactions on Power Electronics*, vol. 38, no. 1, pp. 1336-1347, 2023. <https://doi.org/10.1109/TPEL.2022.3204054>
- [9] H. Feng, A. Dayerizadeh, and S. M. Lukic, "A coupling-insensitive X-type IPT system for high position tolerance," *IEEE Transactions on Industrial Electronics*, vol. 68, no. 8, pp. 6917-6926, 2021. <https://doi.org/10.1109/TIE.2020.3000116>
- [10] P. S. Subudhi, S. Padmanaban, F. Blaabjerg, and D. P. Kothari, "Design and implementation of a PV-fed grid-integrated wireless electric vehicle battery charger present in a residential environment," *IEEE Journal of Emerging and Selected Topics in Industrial Electronics*, vol. 4, no. 1, pp. 78-86, 2023. <https://doi.org/10.1109/JESTIE.2022.3195087>
- [11] F. Grazian, T. B. Soeiro, and P. Bauer, "Voltage/current doubler converter for an efficient wireless charging of electric vehicles with 400-V and 800-V battery voltages," *IEEE Transactions on Industrial Electronics*, vol. 70, no. 8, pp. 7891-7903, 2023. <https://doi.org/10.1109/TIE.2022.3208582>
- [12] Z. Dai, J. Wang, M. Long, H. Huang, and M. Sun, "Magnetic shielding structure optimization design for wireless power transmission coil," *AIP Advances*, vol. 7, article no. 095013, 2017. <https://doi.org/10.1063/1.4990775>
- [13] Z. Dai, J. Wang, H. Zhou, and H. Huang, "A review on the recent development in the design and optimization of magnetic coupling mechanism of wireless power transmission," *IEEE Systems Journal*, vol. 14, no. 3, pp. 4368-4381, 2020. <https://doi.org/10.1109/JSYST.2020.3004201>
- [14] F. Wang, W. Zhang, L. Ye, J. Guo, K. Liu, and H. T. Do, "A design method to implement ZVS for electric vehicle wireless charging system with double-side LCC compensation," *IEEE Journal of Emerging and Selected Topics in Power Electronics*, vol. 9, no. 3, pp. 3791-3801, 2021. <https://doi.org/10.1109/JESTPE.2020.3012614>
- [15] K. Lee and S. H. Chae, "Comparative study of achievable efficiency between three- and four-coil wireless power

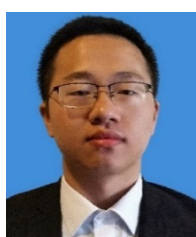
- transfer systems," *IEEE Journal of Emerging and Selected Topics in Power Electronics*, vol. 10, no. 2, pp. 2138-2146, 2022. <https://doi.org/10.1109/JESTPE.2021.3072733>
- [16] W. V. Wang, D. J. Thrimawithana, and M. Neuburger, "An Si MOSFET-based high-power wireless EV charger with a wide ZVS operating range," *IEEE Transactions on Power Electronics*, vol. 36, no. 10, pp. 11163-11173, 2021. <https://doi.org/10.1109/TPEL.2021.3071516>
- [17] J. Tang, T. Na, and Q. Zhang, "A novel full-bridge step density modulation for wireless power transfer systems," *IEEE Transactions on Power Electronics*, vol. 38, no. 1, pp. 41-45, 2023. <https://doi.org/10.1109/TPEL.2022.3200759>
- [18] Z. Dai, W. Peng, Z. Wang, M. Li, Y. Zhou, R. Wang, T. Chen, X. Zhang, and J. Wang, "Reconfigurable receiver with adaptive output voltage for wireless power transfer," *IEEE Transactions on Circuits and Systems I: Regular Papers*, vol. 71, no. 1, pp. 454-462, 2024. <https://doi.org/10.1109/TCSI.2023.3326839>
- [19] Z. Dai, X. Zhang, T. Liu, C. Pei, T. Chen, R. Dou, and J. Wang, "Magnetic coupling mechanism with omnidirectional magnetic shielding for wireless power transfer," *IEEE Transactions on Electromagnetic Compatibility*, vol. 65, no. 5, pp. 1565-1574, 2023. <https://doi.org/10.1109/TEMC.2023.3266089>
- [20] M. Ishihara, K. Umetani, and E. Hiraki, "Strategy of topology selection based on quasi-duality between series-series and series-parallel topologies of resonant inductive coupling wireless power transfer systems," *IEEE Transactions on Power Electronics*, vol. 35, no. 7, pp. 6785-6798, 2020. <https://doi.org/10.1109/TPEL.2019.2956732>
- [21] Z. Dai, J. Wang, M. Long, and H. Huang, "A Witricity-based high-power device for wireless charging of electric vehicles," *Energies*, vol. 10, no. 3, article no. 323, 2017. <https://doi.org/10.3390/en10030323>
- [22] G. Ke, Q. Chen, L. Xu, X. Ren, and Z. Zhang, "Analysis and optimization of a double-sided S-LCC hybrid converter for high misalignment tolerance," *IEEE Transactions on Industrial Electronics*, vol. 68, no. 6, pp. 4870-4881, 2021. <https://doi.org/10.1109/TIE.2020.2988215>
- [23] G. Rituraj and P. Kumar, "A new magnetic structure of unipolar rectangular coils in WPT systems to minimize the ferrite volume while maintaining maximum coupling," *IEEE Transactions on Circuits and Systems II: Express Briefs*, vol. 68, no. 6, pp. 2072-2076, 2021. <https://doi.org/10.1109/TCSII.2020.3044585>
- [24] G. Rituraj, B. K. Kushwaha, and P. Kumar, "A unipolar coil arrangement method for improving the coupling coefficient without ferrite material in wireless power transfer systems," *IEEE Transactions on Transportation Electrification*, vol. 6, no. 2, pp. 497-509, 2020. <https://doi.org/10.1109/TTE.2020.2994091>
- [25] Z. Luo, X. Wei, M. G. S. Pearce, and G. A. Covic, "Multi-objective optimization of inductive power transfer double-D pads for electric vehicles," *IEEE Transactions on Power Electronics*, vol. 36, no. 5, pp. 5135-5146, 2021. <https://doi.org/10.1109/TPEL.2020.3029789>
- [26] M. Mohammad, O. C. Onar, V. P. Galigekere, G. J. Su, and J. Wilkins, "Magnetic shield design for the double-d coil-based wireless charging system," *IEEE Transactions on Power Electronics*, vol. 37, no. 12, pp. 15740-15752, 2022. <https://doi.org/10.1109/TPEL.2022.3191911>
- [27] A. U. Ibrahim, W. Zhong, and M. D. Xu, "A 50-kW three-channel wireless power transfer system with low stray magnetic field," *IEEE Transactions on Power Electronics*, vol. 36, no. 9, pp. 9941-9954, 2021. <https://doi.org/10.1109/TPEL.2021.3064373>
- [28] J. Yi, P. Yang, Z. Li, P. Kong, and J. Li, "Mutual inductance calculation of circular coils for an arbitrary position with a finite magnetic core in wireless power transfer systems," *IEEE Transactions on Transportation Electrification*, vol. 9, no. 1, pp. 1950-1959, 2023. <https://doi.org/10.1109/TTE.2022.3187953>
- [29] Y. P. Su, X. Liu, and S. Y. Hui, "Extended theory on the inductance calculation of planar spiral windings including the effect of double-layer electromagnetic shield," *IEEE Transactions on Power Electronics*, vol. 23, no. 4, pp. 2052-2061, 2008. <https://doi.org/10.1109/TPEL.2008.924824>
- [30] C. M. Zierhofer and E. S. Hochmair, "Geometric approach for coupling enhancement of magnetically coupled coils," *IEEE Transactions on Biomedical Engineering*, vol. 43, no. 7, pp. 708-714, 1996. <https://doi.org/10.1109/10.503178>
- [31] Q. Ke, W. Luo, G. Yan, and K. Yang, "Analytical model and optimized design of power transmitting coil for inductively coupled endoscope robot," *IEEE Transactions on Biomedical Engineering*, vol. 63, no. 4, pp. 694-706, 2016. <https://doi.org/10.1109/TBME.2015.2469137>
- [32] A. K. RamRakhyani, S. Mirabbasi, and M. Chiao, "Design and optimization of resonance-based efficient wireless power delivery systems for biomedical implants," *IEEE Transactions on Biomedical Circuits and Systems*, vol. 5, no. 1, pp. 48-63, 2011. <https://doi.org/10.1109/TBCAS.2010.2072782>

**Zhongyu Dai**<https://orcid.org/0000-0002-4574-405X>

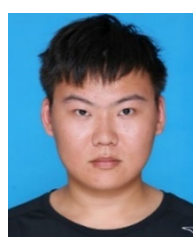
received his B.S. and Ph.D. degrees in electrical engineering from the School of Electrical Engineering and Automation, Wuhan University, Wuhan, P. R. China, in 2014 and 2020, respectively. After this, he joined the School of Power and Mechanical Engineering as a postdoctoral researcher. He is currently an associate professor in the School of Electrical Engineering at Hebei University of Technology. His main research interests include wireless power transmission technology and its applications, and condition monitoring of smart grids.

**Huihui Wang**

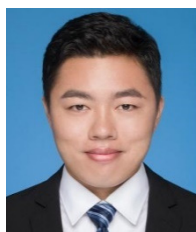
received her B.S. degree in electrical engineering from Shandong Agricultural Engineering University. She is currently working toward her M.E. degree in electrical engineering from Hebei University of Technology, Tianjin, China. Her research interests include wireless power transfer and its industrial applications.

**Wenxi Peng**

received his B.S. degree in electrical engineering from Wuhan University, Wuhan, P. R. China, in 2014. He then joined the State Grid Sichuan Ultra High Voltage Company, where he worked in the field of relay protection. He is currently the leader of the substation maintenance team at State Grid Sichuan Ultra High Voltage Company, as well as a skilled craftsman and young talent recommended by the State Grid Sichuan Electric Power Company. His main research interests include relay protection, professional management, and plan management.

**Yanhu Zhai**

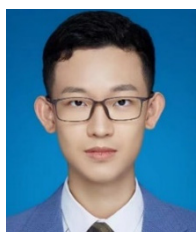
received his B.S. degree in electrical engineering from Shijiazhuang Tiedao University. He is currently working toward his M.E. degree in electrical engineering at Hebei University of Technology, Tianjin, China. His main research interests are wireless power transmission technology and its applications.

**Yake Tang**

received his B.S. and M.S. degrees in electrical engineering from the School of Electrical Engineering and Automation, Wuhan University, Wuhan, P. R. China, in 2015 and 2017, respectively. He is currently an intermediate engineer at the Henan Electric Power Company Economy Research Institute. His main research interests include the design and research of transmission lines.

**Ming Xue**<https://orcid.org/0000-0001-6153-9761>

received his B.S. and M.S. degrees from Tianjin Polytechnic University, Tianjin, China, in 2011 and 2014. In 2022, he received his Ph.D. degree in electrical engineering from the Hebei University of Technology, Tianjin, China. He is currently an associate professor with the School of Electrical Engineering, Hebei University of Technology, Tianjin. His current research interest include wireless power transfer technology and its application.

**Haoran Xu**

is currently working toward his M.E. degree in electrical engineering and automation from Donghua University. His main research interests include the engineering electromagnetic field and power electronics technology.

**Xian Zhang**<https://orcid.org/0000-0002-0925-9831>

received his M.E. and Ph.D. degrees in electrical engineering from Hebei University of Technology, Tianjin, China, in 2009 and 2012, respectively. He is currently a professor at Hebei University of Technology, Tianjin, China. He is the director of the China Electrotechnical Society and the secretary-general of the National Specialized Committee on Wireless Power Transmission Technology. His research interests encompass intelligent high-power wireless power transmission technology, measurement of three-dimensional electromagnetic fields, and numerical calculations of modern engineering electromagnetic fields.